Article

A Comparative Study on CO_2-Switchable Foams Stabilized by C_{22}- or C_{18}-Tailed Tertiary Amines

Meiqing Liang [1], Xuezhi Zhao [2], Ji Wang [1,3,*] and Yujun Feng [1,2,*]

[1] Chengdu Institute of Organic Chemistry, Chinese Academy of Sciences, Chengdu 610041, China; liangmeiqinggucas@126.com
[2] State Key Laboratory of Polymer Materials Engineering, Polymer Research Institute, Sichuan University, Chengdu 610065, China; zhaoxz@scu.edu.cn
[3] Tianfu Yongxing Laboratory, Chengdu 610217, China
[*] Correspondence: coccwangji@hotmail.com (J.W.); yjfeng@scu.edu.cn (Y.F.)

Abstract: The CO_2 aqueous foams stabilized by bioresource-derived ultra-long chain surfactants have demonstrated considerable promising application potential owing to their remarkable longevity. Nevertheless, existing research is still inadequate to establish the relationships among surfactant architecture, environmental factors, and foam properties. Herein, two cases of ultra-long chain tertiary amines with different tail lengths, *N*-erucamidopropyl-*N*,*N*-dimethylamine ($UC_{22}AMPM$) and *N*-oleicamidopropyl-*N*,*N*-dimethylamine ($UC_{18}AMPM$), were employed to fabricate CO_2 foams. The effect of temperature, pressure and salinity on the properties of two foam systems (i.e., foamability and foam stability) was compared using a high-temperature, high-pressure visualization foam meter. The continuous phase viscosity and liquid content for both samples were characterized using rheometry and FoamScan. The results showed that the increased concentrations or pressure enhanced the properties of both foam samples, but the increased scope for $UC_{22}AMPM$ was more pronounced. By contrast, the foam stability for both cases was impaired with increasing salinity or temperature, but the $UC_{18}AMPM$ sample is more sensitive to temperature and salinity, indicating the salt and temperature resistance of $UC_{18}AMPM$-CO_2 foams is weaker than those of the $UC_{22}AMPM$ counterpart. These differences are associated with the longer hydrophobic chain of $UC_{22}AMPM$, which imparts a higher viscosity and lower surface tension to foams, resisting the adverse effects of temperature and salinity.

Keywords: CO_2 aqueous foams; foam properties; ultra-long chain surfactants; CO_2-switchable; surface tension

1. Introduction

Carbon dioxide (CO_2) aqueous foams are colloidal dispersions composed of CO_2 bubbles dispersed in a continuous aqueous phase [1]. Due to their relatively low density, larger surface area and excellent fluidity, CO_2 aqueous foams have been widely used in many industrial processes and applications including the petroleum industry [2], ore flotation [3] and firefights [4]. The traditional CO_2 aqueous foams were obtained using anionic surfactants such as sodium dodecyl sulfate (SDS) [5] and alpha olefin sulfonate (AOS) [6] as foaming agents by decreasing the CO_2–water interfacial tension (C–W IFT) and capillary forces (P_c). Unfortunately, such CO_2 aqueous foams rapidly destabilized through a combination of drainage [7,8], coalescence [7,8], and Ostwald ripening [9]. As a result, the lifetime CO_2 aqueous foams made of common surfactants do not exceed a few tens of minutes [10,11] and fail to satisfy the practical requirements. To improve foam lifetime, various foam stabilizers, including polymer [12,13], protein [14–16], and nanoparticles [17,18], are introduced into the aqueous foam systems against foam destabilization. In some cases, there is a demand for both the stable foam formed and controlled foam destruction. Taking

cleaning processes as an example, the stable foam needs to be destabilized rapidly in a controlled way at the end of cleaning to obtain only a small volume of contaminated liquid that is easier to handle compared with foam [19]. Therefore, switchable or stimuli-responsive foams with tunable stability have been paid much attention in recent years.

During the past decade, the use of bioresource-derived ultra-long-chain surfactants (the hydrophobic chains $\geq C_{18}$) as stabilizers to prepare long-lasting aqueous foams has been widely reported and attracted significant interest. Johnston et al. [20] pioneered the utilization of erucylamidopropyldimethyl betaine (EAPB) to prepare long-lived CO_2 foams. The CO_2 foams stabilized by EAPB are intact at temperatures up to 120 °C and CO_2 volumetric fractions up to 0.98. Likewise, our laboratory used *N*-erucamidopropyl-*N*,*N*-dimethylamine ($UC_{22}AMPM$) to develop a CO_2 aqueous foam with a lifetime of up to 6 h in 120 °C and 10 MPa [21]. The mechanism behind the foams stabilization by ultra-long-chain surfactants can be summarized as follows: (i) ultra-long-chain surfactants adsorb at CO_2–water interfaces to form a dense surfactants layer in foam film, resisting coarsening and coalescence of bubbles [22]; (ii) the ultra-long-chain surfactants can assemble into viscoelastic aggregates, enhancing the solution viscosity and thus suppressing the liquid drains within the foam film [23,24]. In addition to their excellent foam stabilization capability, another merit of ultra-long-chain surfactants over petrochemical-based short-chain surfactants is being environmentally benign and sustainable as their feedstocks are natural renewable materials such as vegetable oil [25,26]. To provide scientific guidance for the application of CO_2 foams in harsh conditions, previous research on ultra-long-chain surfactants stabilizing CO_2 aqueous foams has been focused on establishing the relationships between various factors (e.g., pH, temperature, salinity and pressure) and foam properties [21,27]. However, these studies have typically been conducted in a single foam system, mainly rooted in the previous view that foam destabilization depends more on the mesoscopic properties of the foam such as bubble radius, foam film thickness and liquid fraction than on the chemical properties of the surfactant. Consequently, there are still insufficient insights into the contribution of surfactant structure to foam stability and evolution, impeding the advancement and exploitation of such foam systems.

In fact, many studies have demonstrated that surfactant structure has a noticeable impact on foam evolution and stability [16,28,29]. Fameau et al. [30] explored the role of tail length and head groups in foam properties by comparing the performance of foams made from long-chain fatty acids (myristic acid, palmitostearic acid, juniperic acid and 12-hydroxystearic acid). They found the foamability of fatty acid-based foam increased with decreasing the alkyl chain length of the fatty acid. Moreover, the presence of a hydroxyl group on the hydrophobic tail of the fatty acids increases the foamability in comparison to the non-hydroxylated fatty acids analog. A systematic study of foams made with a series of multi-tailed surfactants reported by Feitosa and co-workers demonstrated foams made with tri-cephalic double-tailed molecules have better stability than the single-tail one, regardless of the head structure [10]. Enlightened by these findings, we can safely hypothesize that aqueous foams stabilized by ultra-long-chain surfactants with different structures will exhibit differentiated foam properties and aging processes. In this context, it is desirable and beneficial to establish the correlation among the molecular structure of long-tailed surfactants, foam properties and evolution.

The objective of this study is to establish the surfactant structure-foam properties-foam evolution links and to deepen the understanding of the role of surfactant structure in foam properties. To attain this goal, $UC_{22}AMPM$ and its analog ($UC_{18}AMPM$, C_{18} tail, Scheme 1) were used as model compounds to develop CO_2 aqueous foams. Then, the foaming ability and foam stability of two CO_2 aqueous foam systems were meticulously compared at various temperatures, pressures and salinity using FoamScan and a high-temperature, high-pressure (HTHP) visualization foam meter. Meanwhile, the as-prepared CO_2 aqueous foams were investigated by rheometer to unravel the underlying principles driving the discrepancies in foam properties.
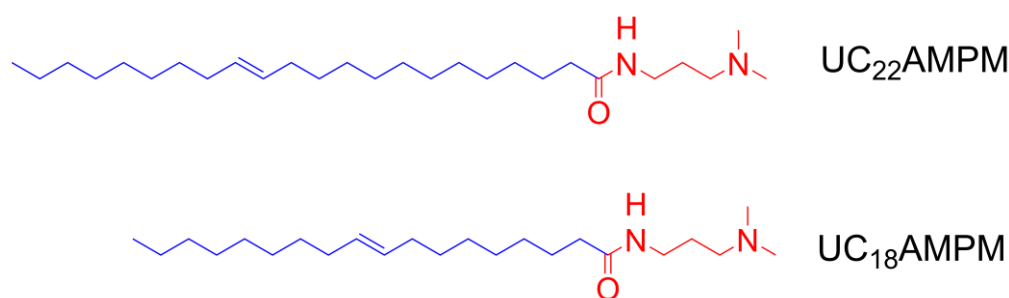
Scheme 1. The chemical structures of *N*-erucamidopropyl-*N,N*-dimethylamine (UC$_{22}$AMPM) and *N*-oleicamidopropyl-*N,N*-dimethylamine (UC$_{18}$AMPM).

2. Results and Discussion

The section is organized as follows: First, the concentration of UC$_{22}$AMPM and UC$_{18}$AMPM is optimized by the static foam test in atmospheric pressure at 35 °C. Then, the switching behavior of UC$_{18}$AMPM-CO$_2$ aqueous foam is characterized in comparison with UC$_{22}$AMPM-CO$_2$ aqueous foam. Finally, the influence of temperature, salinity, and pressure on the performance of CO$_2$ aqueous foams UC$_{22}$AMPM and UC$_{18}$AMPM is examined, respectively.

2.1. Determination of Optimum Concentration

It is known that foam properties strongly depend on the concentration of the foaming agent [31,32]. Generally, the foaming properties are referred to as foamability (the maximum volume of foam system for a certain volume of foaming agent solution after a certain time of shear effect at a certain temperature, V$_{max}$) [33,34] and foam stability (the time taken by the volume of foam system from V$_{max}$ to a half at a certain temperature, t$_{1/2}$) [33,34]. To determine the optimum concentration, the properties of UC$_{22}$AMPM and UC$_{18}$AMPM foams were investigated separately as a function of the concentration (0.1–0.5%) using FoamScan under atmospheric pressure at 35 °C. We previously demonstrated that UC$_{22}$AMPM could form stable CO$_2$ aqueous foams but not N$_2$ ones [21,35]. Thus, CO$_2$ was employed as the foaming gas in this work.

Figure 1A,B present the changes in V$_{max}$ and t$_{1/2}$ of both aqueous foams with increasing concentration, respectively. It can be seen the V$_{max}$ for UC$_{18}$AMPM was always constant at around 180 mL with increasing UC$_{18}$AMPM concentration ($C_{UC18AMPM}$), while the V$_{max}$ of UC$_{22}$AMPM rose from 179 to 189 mL (Figure 1A). Meanwhile, the t$_{1/2}$ of both aqueous foams rose as the concentration increased (Figure 1B). From Table 1, the t$_{1/2}$ of UC$_{22}$AMPM-CO$_2$ aqueous foams improved by 2.6 fold as the concentration of UC$_{22}$AMPM ($C_{UC22AMPM}$) increased from 0.1% to 0.5%, higher than the increment factor of UC$_{18}$AMPM-CO$_2$ aqueous foams (~1.6). These results indicated that the $C_{UC22AMPM}$ exerts a more prominent influence on foamability and foam stability compared to $C_{UC18AMPM}$.

The foam comprehensive index (FCI) [6], a quantitative measure to assess the foam properties, was employed to calculate the optimal concentration. The FCI can be expressed below [36]:

$$\text{FCI} = \int_0^{t_{1/2}} \text{V} dt = \frac{3}{4} V_{max} t_{1/2} \tag{1}$$

As listed in Table 1, the FCI of UC$_{22}$AMPM and UC$_{18}$AMPM reached maximum values of 1,382,062 s·mL and 49,140 s·mL at a concentration of 0.5 wt.%, respectively. Typically, the value of FCI is greater, the foam properties are better [37]. Based on the FCI criterion, 0.5 wt.% as the optimal UC$_{22}$AMPM and UC$_{18}$AMPM concentration was used in the following experiments. Furthermore, we also concluded that the 0.5% UC$_{22}$AMPM has superior foam properties to 0.5% UC$_{18}$AMPM.
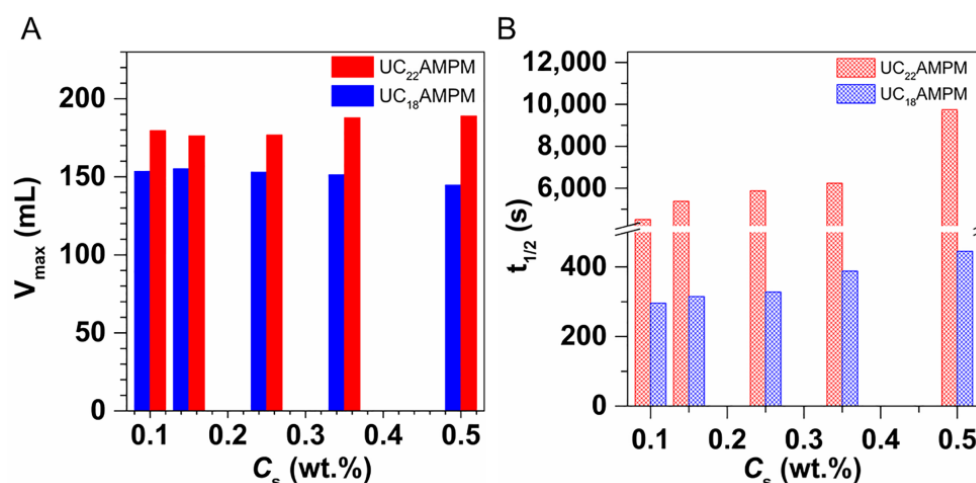
Figure 1. The influence of surfactant concentrations on (**A**) V_{max} and (**B**) $t_{1/2}$ of $UC_{22}AMPM$ and $UC_{18}AMPM$ in atmospheric pressure at 35 °C, respectively.

Table 1. CO_2 foam performance with different concentrations of $UC_{22}AMPM$ and $UC_{18}AMPM$, respectively.

	C_s (wt.%)	$t_{1/2}$ (s)	V_{max} (mL)	FCI (s·mL)
	0.1	296	153	33,621
	0.15	315	155	36,618
$UC_{18}AMPM$	0.25	328	153	37,638
	035	388	151	43,941
	0.5	445	144	49,140
	0.1	4509	179	605,333
	0.15	5379	176	710,028
$UC_{22}AMPM$	0.25	5872	176	775,104
	035	6240	187	879,372
	0.5	9750	189	1,382,062

To shed light on the reasons behind the difference in properties between $UC_{22}AMPM$ and $UC_{18}AMPM$ foams at their optimum concentration, the foam evolution process, liquid content (φ) of aqueous foams (the ratio of the liquid volume to the foam volume) and continuous phase viscosity (η) of foam bulk phase were studied. As shown in Figure 2, the geometry of the bubble is spherical for both cases at the initial moment (30 s). For $UC_{22}AMPM$ foams, there was virtually no change in the bubble morphology as time progressed. In contrast, the bubbles in $UC_{18}AMPM$ aqueous foams evolved quickly into irregular polyhedral over time. At the 540th second, a substantial number of bubbles of $UC_{18}AMPM$ aqueous foams disappeared, indicative of foam bursting. In principle, the bubble shape is dependent on the φ of the aqueous foam [8]. In the case of high φ in the aqueous foams, the bubbles are uniformly spherical and densely packed. Decreasing the φ causes bubble deformation and the formation of defined edges. Therefore, we can conclude that the φ of $UC_{22}AMPM$ foams remain constant for 540 s, indicative of slow drainage. In the case of $UC_{18}AMPM$ foams, the faster bubble deformation could be interpreted by the rapid lowering of φ, resulting from the acceleration of the drainage process. From optical visualization, we could draw a conclusion that the foam drainage process of $UC_{22}AMPM$ foams is weaker than that of $UC_{18}AMPM$ foams.
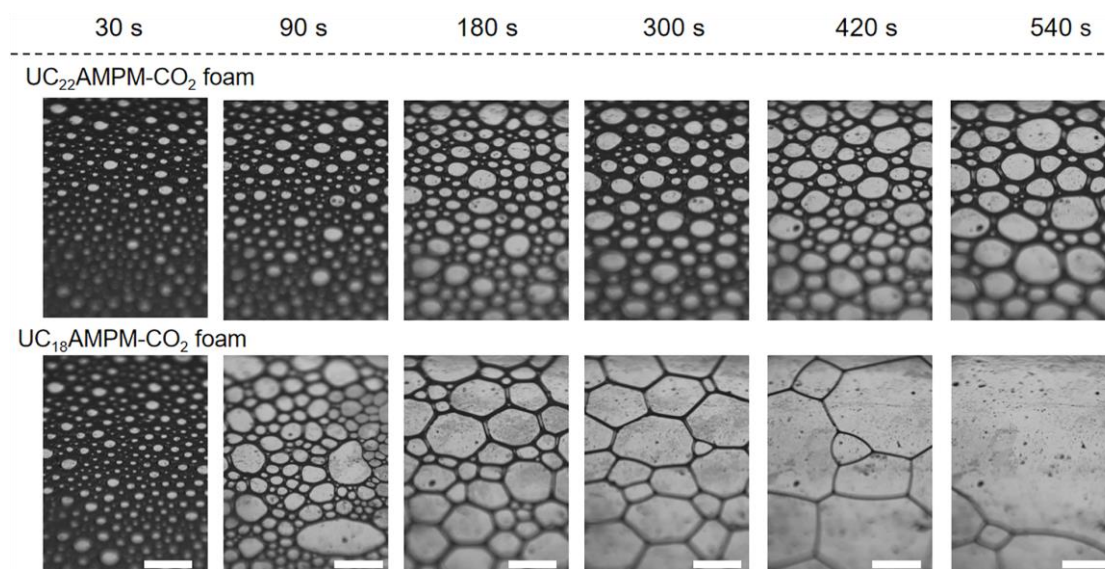
Figure 2. Comparison of morphology evolution of CO_2 aqueous foams made from 0.5% $UC_{22}AMPM$ and 0.5% $UC_{18}AMPM$ with time in atmospheric pressure at 35 °C.

The variation in the φ as a function of time is shown in Figure 3A. Evidently, the φ in both cases increased significantly over time during the generation process of aqueous foams, reaching a maximum liquid content (φ_m) on completion of foaming. Comparatively speaking, the φ_m of the 0.5% $UC_{22}AMPM$-CO_2 aqueous foams was about 24.7%, greater than that of the 0.5% $UC_{18}AMPM$-CO_2 aqueous foams (10.6%). The lower φ_m is associated with its V_{max} (145 mL), indicative of the inferior foaming ability of $UC_{18}AMPM$. As is well-known, the foamability is positively proportional to the C-W IFT (γ) of the surfactant solution, which can be described by using the previously reported [38]:

$$W = \gamma A \tag{2}$$

here W and A stand for external energy applied to generate the foam and the foam area created, respectively. For a fixed W, the higher the γ is, the lower the V_{max} will be. On the basis of a previous study by Feng et al. [39], with the identical head group, the γ increases with the decrease in the hydrophobic chain length. One can conclude that the γ of the $UC_{18}AMPM$-CO_2 solution is higher than that of the $UC_{22}AMPM$ counterpart due to its shorter alkyl chain. Thus, the $UC_{18}AMPM$-CO_2 solution presents poor foamability as compared with the $UC_{22}AMPM$ counterpart.

Upon CO_2 sparging cease, the φ reduced gradually with time because of the drainage. It can be seen that the $UC_{18}AMPM$-CO_2 aqueous foams drained in the 200s to $\varphi = 0$, while the φ of $UC_{22}AMPM$-CO_2 aqueous foam was 20% in this period (Figure 3A), demonstrating that the drainage from $UC_{18}AMPM$-CO_2 aqueous foams is faster than that of $UC_{22}AMPM$-CO_2 aqueous solution.

The rheological results demonstrated the $UC_{22}AMPM$ dispersion saturated with CO_2 attained very high values of zero-shear viscosity η_o (3.75×10^4 mPa·s) and showed shear-thinning behavior (Figure 3B). The high magnitude of η_o mirrors the presence of entangled wormlike micelles in solution [40,41]. In contrast, the η_o for $UC_{18}AMPM$ samples was only ~1.0 mPa·s (Figure 3B), reflecting the absence of wormlike micelles. Numerous studies have established that drainage velocity (V) should vary inversely with the viscosity of the continuous phase (η), as the following equation [42]:

$$V = \frac{dh_f}{dt} = \frac{h_f^3}{3\eta R_f^2} \Delta P_{film} \tag{3}$$

where ΔP_{film} stands for the difference in pressure between the film center and border, h_f refer to the thickness of the thin film. Using Equation (3), one can conclude that the V of $UC_{18}AMPM$-CO_2 aqueous foams is four orders of magnitude greater than that of $UC_{22}AMPM$-CO_2 aqueous foams, consistent with our earlier conclusion (Figure 2). The consequence of faster drainage is that the φ decreases rapidly, concomitant with the reduction in film thickness. The thin films tend to rupture, leading to rapid foam destruction. As a result, $UC_{18}AMPM$-CO_2 aqueous foams show a $t_{1/2}$ of 445 s, which is much shorter relative to $UC_{22}AMPM$-CO_2 aqueous foams (9750 s) in identical conditions.
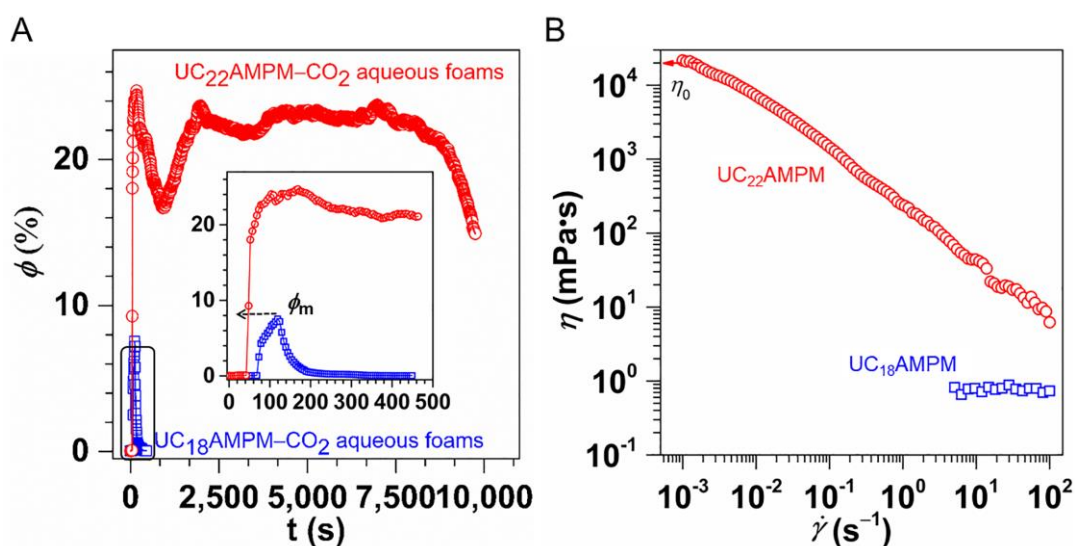

Figure 3. (**A**) Variation of the liquid content (φ) for 0.5% $UC_{22}AMPM$ and 0.5% $UC_{18}AMPM$ as a function of time. (**B**) Shear viscosity (η) plotted as a function of shear rate for 0.5% $UC_{22}AMPM$ and 0.5% $UC_{18}AMPM$ solutions at 35 °C.

According to the aforementioned results, we attributed the differences in performance between $UC_{22}AMPM$ and $UC_{18}AMPM$ foams to their viscosity discrepancy, rooted in the different assembled structures of $UC_{22}AMPM$ and $UC_{18}AMPM$. More specifically, $UC_{22}AMPM$ with 0.5% concentration can self-assemble into wormlike micelles, but $UC_{18}AMPM$ cannot. For the $UC_{22}AMPM$ system, the entangled worm-like micelles impart high viscosity to the foam continuous phase. During the foaming process, a large amount of liquid was transported into the foam liquid channels, forming thick foam films. The thick films would increase the thermal activation energy barrier against coalescence and Ostwald ripening. More important, the drainage is retarded by high η. Overall, high continuous phase viscosity retarded the three types of foam destabilization processes simultaneously, thereby enhancing the stability of foams. In contrast, the $UC_{18}AMPM$ behaved as a low η Newtonian fluid due to the absence of wormlike micelles, leading to the formation relatively thin foam film. Furthermore, lamellae films drained rapidly due to the low η of the aqueous phase. The consequence of faster drainage is that the foam film becomes thinner and prone to rupture, leading to foam destruction. Therefore, the $UC_{18}AMPM$-CO_2 solution presents poor foam properties as compared with the $UC_{22}AMPM$ counterpart.

2.2. A Comparison of the Foams Switchability

We previously demonstrated the aqueous foams stabilized by $UC_{22}AMPM$ could be turned "on" and "off" on demand through the bubbling of CO_2 or adding $NH_3 \cdot H_2O$. It is essential to examine the switchability of the $UC_{18}AMPM$-CO_2 foam and to make a comparison with the $UC_{22}AMPM$ ones. The pressure and temperature are constant at 3 MPa and 80 °C, respectively, to ensure that the above two compounds can be protonated again after the neutralization of $NH_3 \cdot H_2O$.

Figure 4 depicts the parallel variations of V_{max} and $t_{1/2}$ of both CO_2 foam systems after the alternating addition of $NH_3 \cdot H_2O$ and CO_2. It was apparent that the $t_{1/2}$ rose or declined accordingly with the alternative introduction of CO_2 and $NH_3 \cdot H_2O$, suggesting the foam lifetime of both foam systems can be reversibly tuned. This finding proved that CO_2 aqueous foams prepared from $UC_{18}AMPM$ feature switchability similar to UC22AMPM, resulting from their identical hydrophilic headgroups. As shown in Scheme 2, both $UC_{22}AMPM$ and $UC_{18}AMPM$ in water can be protonated into cationic surfactants after sparging CO_2, lowering C-W IFT by adsorbing at the CO_2/water interface and thereby promoting foam formation. Upon $NH_3 \cdot H_2O$ addition, protonated surfactant converted to a surface-inactive neutral form. Consequently, $UC_{22}AMPM$ and $UC_{18}AMPM$ would desorb from the CO_2/water interface, disrupting the foam film and thereby leading to rapid foam destabilization.
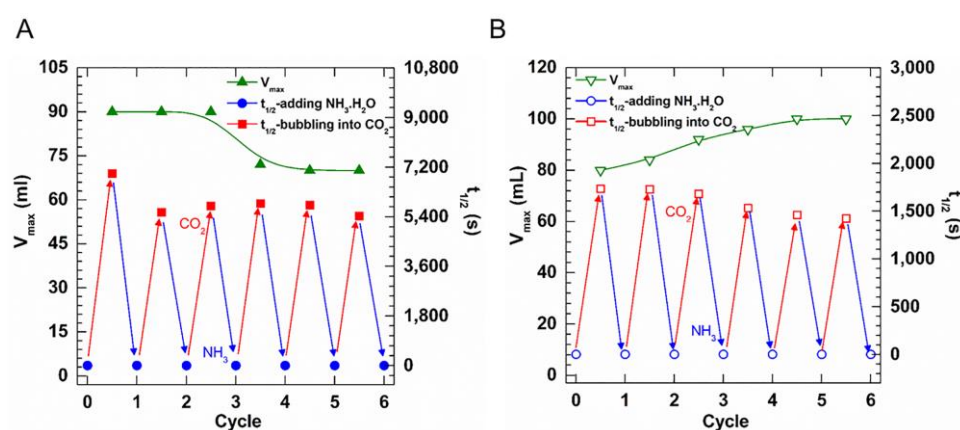

Figure 4. Variation in V_{max} and $t_{1/2}$ of (**A**) 0.5% $UC_{22}AMPM$ and (**B**) 0.5% $UC_{18}AMPM$ foams treated with CO_2 followed by $NH_3 \cdot H_2O$, respectively.

Notably, the V_{max} of $UC_{22}AMPM$-CO_2 foams initially remained constant and then gradually declined as the cycle number increased (Figure 4A), demonstrating foamability weakening. By comparison, the V_{max} of $UC_{18}AMPM$-CO_2 foams gradually boosted as the foaming/defoaming cycle number increased (Figure 4B), indicative of enhanced foamability. On the other hand, the $t_{1/2}$ of both CO_2 foam systems decreased as the number of foaming/defoaming cycles increased (Figure 4A,B), indicating that foam stability deteriorated as the cycle number increased. A similar result was observed in our earlier studies, arising from the accumulation of by-products (a mixture of ammonium carbonate and bicarbonate) [21].

n =18　R = $-(CH_2)_8CH=CH(CH_2)_7CH_3$

n =22　R = $-(CH_2)_{11}CH=CH(CH_2)_7CH_3$
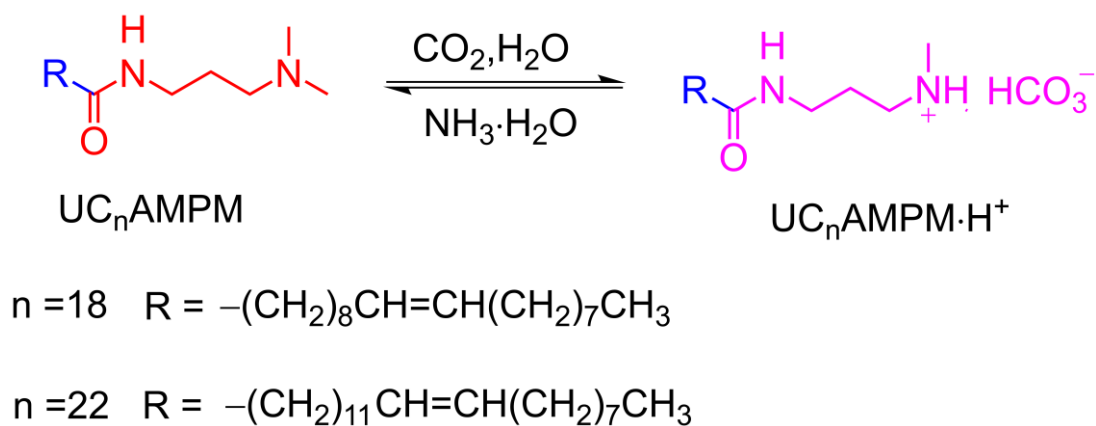
Scheme 2. The protonation of $UC_{22}AMPM$ or $UC_{18}AMPM$ in the presence of CO_2 and H_2O at 80 °C, 3 MPa.

2.3. Comparison of the Effect of External Factors on Foam Properties

It has been recognized that external factors such as temperature, pressure and salinity can significantly affect the foam properties [21]. In the following subsections, the influence of these external factors on the properties of the above two CO_2 aqueous foams was investigated comparatively using an HTHP visualization foam meter.

2.3.1. Effect of Temperature

To examine the impact of temperature on the CO_2 aqueous foams made with $UC_{22}AMPM$ or $UC_{18}AMPM$, $t_{1/2}$ and V_{max} were determined in a temperature range of 25–120 °C at a constant pressure of 3 MPa. As shown in Figure 5A, the V_{max} of both foams systems increased slightly with the temperature elevated, meaning that the increment of temperatures improves the foaming ability.
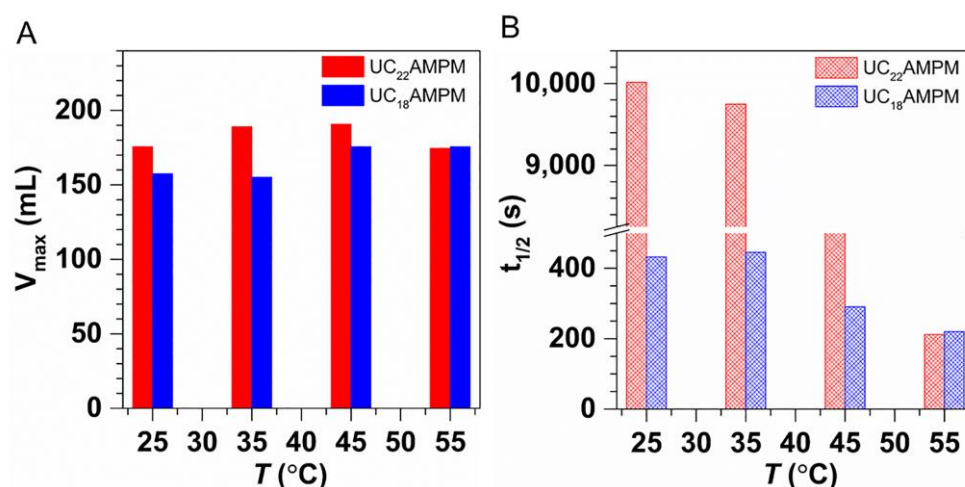

Figure 5. The (**A**) V_{max} and (**B**) $t_{1/2}$ of 0.5% $UC_{22}AMPM$ dispersion and 0.5% $UC_{18}AMPM$ dispersion plotted as a function of temperature at 3 MPa in the presence of CO_2, respectively.

Compared in Figure 5B are the changes in $t_{1/2}$ for the above two aqueous foams systems at different temperatures. Both foam systems displayed similar evolution trends, i.e., the $t_{1/2}$ diminished steeply with the elevation of temperature, demonstrating that increased temperature would deteriorate foam stability. Many studies have revealed the elevating temperature resulted in increased C-W IFT [22] and decreased η [40] at constant pressure. Therefore, the foam destabilization accelerates with increasing temperature as a consequence of the higher C-W IFT and lower η, leading to poor foam stability.

Note also that the $t_{1/2}$ of $UC_{22}AMPM$-CO_2 aqueous foams is greater than that of $UC_{18}AMPM$-CO_2 aqueous foams within the studied temperature scope, signifying that the CO_2 aqueous foam stabilized by $UC_{22}AMPM$ exhibits better temperature resistance compared to $UC_{18}AMPM$ foams. In addition, the $t_{1/2}$ of $UC_{22}AMPM$-CO_2 aqueous foams diminished by 5.3 fold when temperature increased from 25 to 120 °C, smaller than that of the $UC_{18}AMPM$-CO_2 aqueous foams (~9 fold), illustrating the impact of temperature on the stability of $UC_{18}AMPM$-CO_2 aqueous foams is more prevalent related to $UC_{22}AMPM$. One explanation here could be that the P_c is higher than that of $UC_{18}AMPM$ due to its relatively lower φ.

2.3.2. Effect of Pressure

As observed in Figure 6A,B, the V_{max} and $t_{1/2}$ for both samples increased with the increasing pressure, demonstrating that increasing pressure is conducive to foaming ability and foam stability. The finding is consistent with previous studies [21,43,44] attributed to the decrease in the C−W IFT with the pressure increasing. Specifically, high pressure enhances the interactions between CO_2 and the hydrophobic tail of surfactant molecules, reducing the contact probability between CO_2 and water molecules and thus generating

a lower C-W IFT [44]. Clearly, a lower C-W IFT enables the foam to easier form and to mitigate the foam aging process.
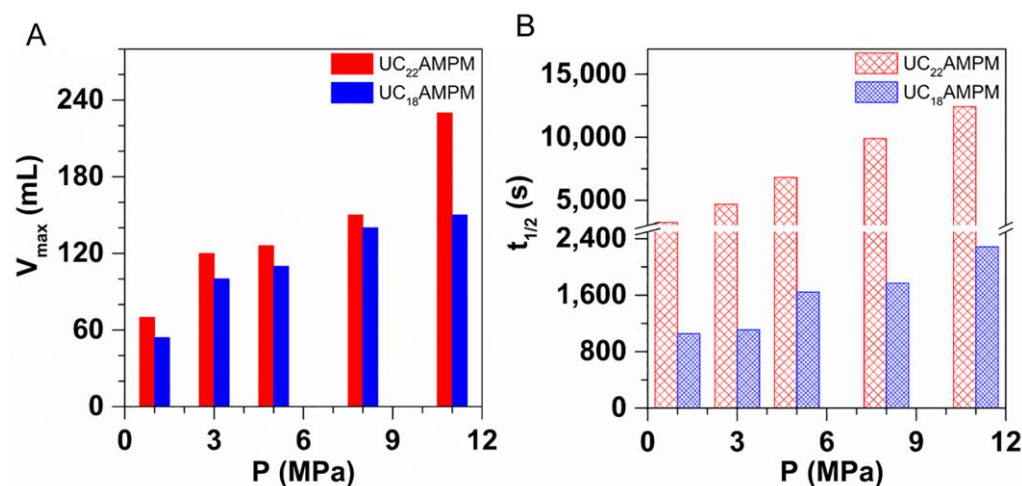

Figure 6. The influence of pressure on (**A**) V_{max} and (**B**) $t_{1/2}$ of 0.5% $UC_{22}AMPM$-CO_2 solution and 0.5% $UC_{18}AMPM$-CO_2 solution, respectively. The experimental temperature is fixed at 120 °C.

Interestingly, the increased scope of V_{max} of both foams showed a similar variation tendency with increasing pressure. The V_{max} for $UC_{22}AMPM$-CO_2 aqueous foam increased from 70 to 230 mL at the tested pressures scope; the $UC_{18}AMPM$-CO_2 aqueous foam increased from 54 and 150 mL under identical conditions. Their V_{max} increased by approximately three times, suggesting the effect of pressure on the foaming ability of both compounds is identical. Instead, the $t_{1/2}$ for $UC_{22}AMPM$-CO_2 aqueous foam increased from 3200 and 12,400 s, showing a faint increase; while the $t_{1/2}$ of $UC_{18}AMPM$-CO_2 aqueous foam underwent a slight increase from 1000 to 2200 s. The growth fold of $t_{1/2}$ for $UC_{22}AMPM$-CO_2 aqueous foam is around 3.9, higher than that of $UC_{18}AMPM$ ones (2.2). These results highlighted that pressure is more prominent in enhancing the stability of $UC_{22}AMPM$-CO_2 aqueous foam compared with that of $UC_{18}AMPM$-CO_2 aqueous foam.

2.3.3. Effect of Salinity

Inorganic salts have been found to modulate the surface activities [45], altering the properties of the surfactant-stabilized foam [43]. Hence, a common sodium chloride (NaCl) was used as representative inorganic salt to add the above two foam systems to clarify the effect of salt on the properties of $UC_{22}AMPM$ and $UC_{18}AMPM$ CO_2 aqueous foams.

As depicted in Figure 7A, the V_{max} of both foams samples increased initially and then maintained constant with increasing NaCl concentration. For example, the $UC_{18}AMPM$ foam expanded from 151 and 175 mL when NaCl concentration increased from 0 to 1 wt.%; while the $UC_{22}AMPM$ foam slightly grew from 189 and 199 mL by increasing NaCl concentration from 0 to 0.5 wt.%. This means that the addition of a small amount of NaCl is beneficial for foamability. A plausible explanation could be that the addition of NaCl enhanced the adsorption of surfactant molecules at the C-W interface as a result of the charge neutralization, leading to the reducing C-W IFT, and thereby improving foaming ability [46]. Thereafter, the V_{max} of both samples remained virtually constant with a further increase in NaCl concentration. We believe that electrostatic repulsions between surfactants are sufficiently shielded at high NaCl content ($\geq$1.0 wt.%). In this scenario, the surfactants were saturated in CO_2/water interfaces, and the C-W IFT achieved a minimum value. Consequently, high NaCl concentrations have a negligible effect on foamability.
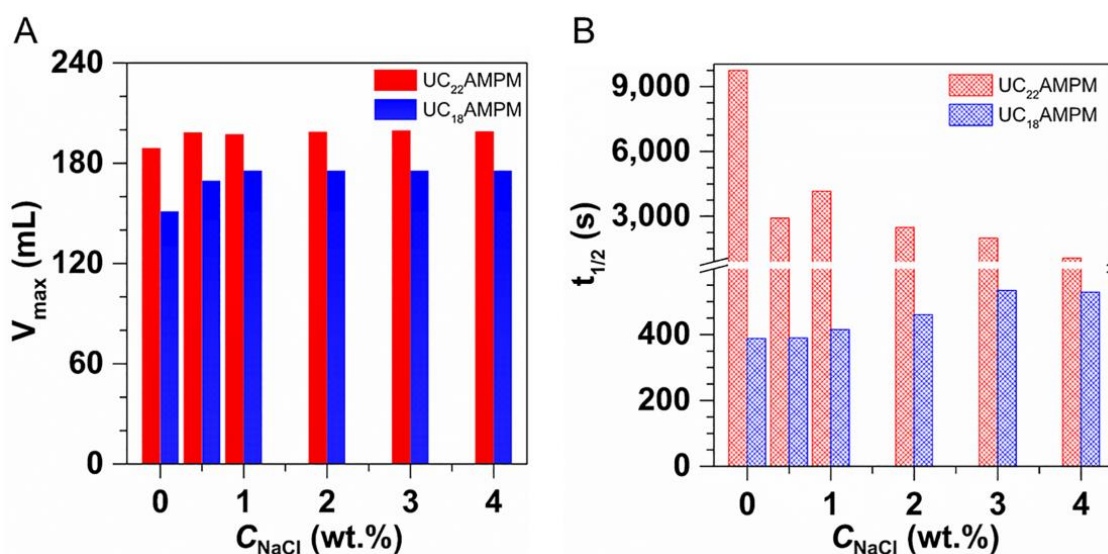
Figure 7. Comparison of the effect of NaCl concentrations on (**A**) V_{max} and (**B**) $t_{1/2}$ of 0.5% $UC_{22}AMPM$-CO_2 solution and 0.5% $UC_{18}AMPM$-CO_2 solution, respectively, at 35 °C under atmospheric pressure.

Compared in Figure 7B is the $t_{1/2}$ for two cases of CO_2 aqueous foams as a function of NaCl concentration. Overall, the $t_{1/2}$ of the $UC_{22}AMPM$ foam samples showed a downtrend at the tested NaCl concentrations, manifesting that the addition of NaCl undermined the foam stability of $UC_{22}AMPM$. This can be interpreted with the fact that the additional NaCl causes a transformation from linear to branched micelles, leading to a decrease in η [47,48]. Upon the decrease in η, the foam aging process would speed up, leading to rapid foam destruction. As for CO_2 aqueous foams made from $UC_{18}AMPM$, $t_{1/2}$ gradually increased and then remain unchanged with increasing salinity. We also attributed this enhanced $t_{1/2}$ to the fact that the presence of NaCl enhances the adsorption density of surfactant molecules on the CO_2/water interface through electrostatic screening, enhancing the strength of foam lamella and therefore resisting gas diffusion between bubbles.

It is also noteworthy that the $t_{1/2}$ of $UC_{22}AMPM$-CO_2 aqueous foams is higher than that of $UC_{18}AMPM$-CO_2 aqueous foams within the studied salinity scope, signifying that the CO_2 aqueous foam stabilized by $UC_{22}AMPM$ exhibits better salt tolerance compared to $UC_{18}AMPM$ foams.

3. Materials and Methods

3.1. Materials

$UC_{18}AMPM$ and $UC_{22}AMPM$ were synthesized according to our previously-reported procedure [39] and confirmed by proton nuclear magnetic resonance spectroscopy (^{1}H NMR, Figures 8 and 9). CO_2 (≥99.998%) was purchased from Jinnengda Gas Company (Chengdu, China) and was used as received. Sodium chloride (NaCl, 99%, GC) and $NH_3 \cdot H_2O$ (25 Vol.%) were purchased from Chengdu Kelong Chemical Factory Co., Ltd. (China). CD_3Cl (≥98% deuterium content) used for ^{1}H NMR analysis was obtained from Sigma-Aldrich (Shanghai, China). The deionized water with a resistivity of 18.25 MΩ·cm used throughout this study was prepared from a quartz water purification system (UPH-I-10T, Chengdu Ultra-pure Technology Co., Ltd., Chengdu, China).
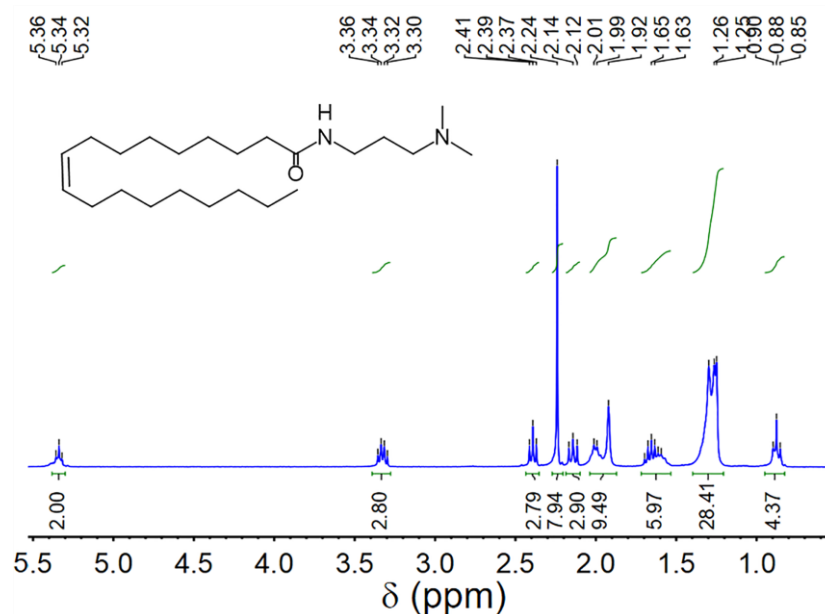
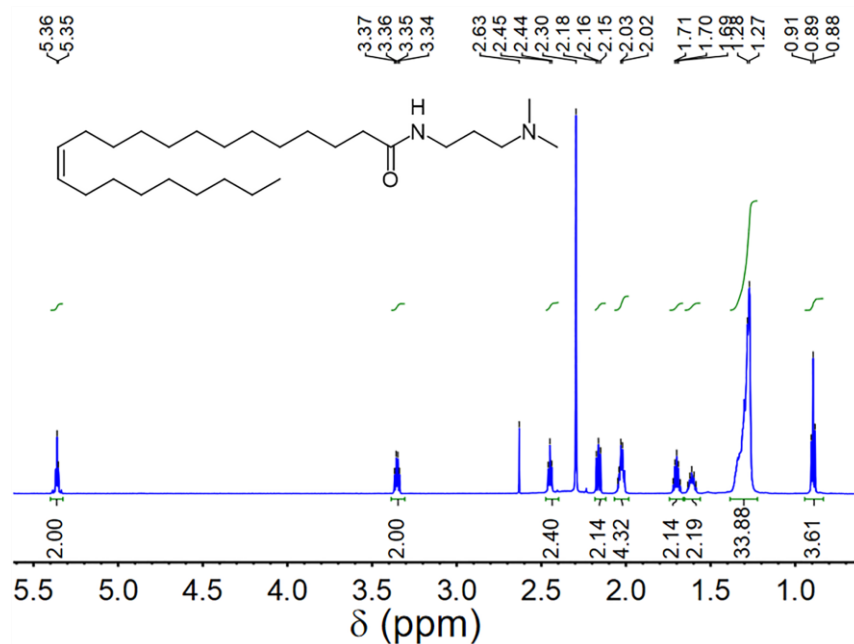**Figure 8.** ^{1}H NMR spectrum of UC$_{18}$AMPM (400 MHz, CDCl$_3$).

Figure 9. ^{1}H NMR spectrum of UC$_{22}$AMPM (400 MHz, CDCl$_3$).

3.2. Preparation of Foaming Solution

A concentrated parent dispersion was prepared by adding designed amounts of surfactant samples (UC$_{22}$AMPM or UC$_{18}$AMPM) and deionized water to a sealed Schott-Duran bottle equipped with a magnetic bar inside. Next, the resulting mixture was stirred at 60 °C for at least 10 min, yielding low-viscosity emulsion-like dispersion. Remarkably, the dispersion concentration was calibrated by adding water to compensate for the water evaporation during the agitation process. The parent dispersions were cooled to room temperature. Then, the dispersions with desired concentration were obtained by diluting the concentrated parent dispersion with deionized water or brine.

3.3. Evaluation of Aqueous Foams at Atmospheric Pressure

The FoamScan setup (Figure 10, TECLIS, Lyon, France), which combines image analysis and conductivity measurements to monitor foam properties, was employed to characterize the foam properties of two types of ultra-long chain tertiary amines (i.e., $UC_{22}AMPM$ and $UC_{18}AMPM$). Briefly, 60 mL of dispersions were placed in the glass column with a porous glass filter (pore diameter 0.2 mm) and heated to the desired temperature by an embedded electric heating system. The pressure of the chamber was fixed at atmospheric pressure. Afterward, aqueous foams were formed by bubbling CO_2 for two minutes. The CO_2 flow rate is constant at 100 mL/min by mass flow meters. The foam volume and liquid content were measured by five pairs of electrodes located along the glass column. The bubbles evolution was captured by the CCD (charge-coupled device) camera after the gas flow stopped.
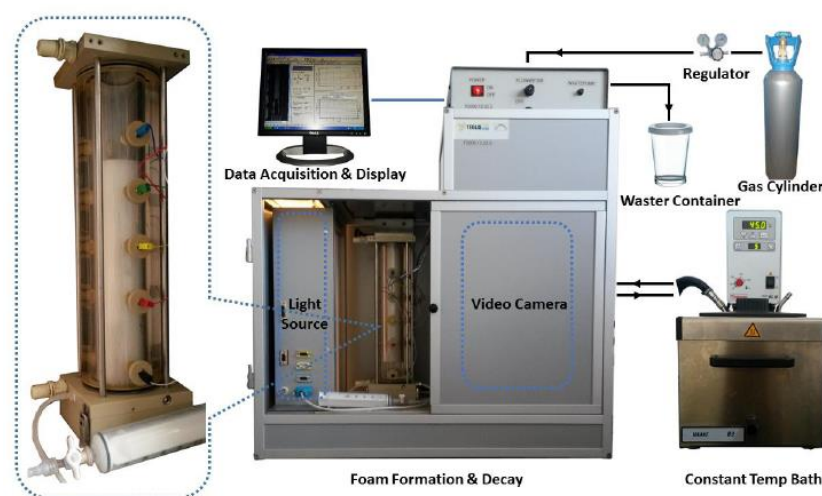

Figure 10. A schematic diagram of FoamScan setup.

3.4. Evaluation of Aqueous Foams at High Pressure

Given that the FoamScan cannot perform at high pressure, the foam properties under high-pressure conditions were evaluated by an HTHP visualization foam meter (Jiangsu Hongbo Machinery Manufacturing Co., Ltd., Haian China). A detailed description of the HTHP visualization foam meter and operating procedures have been reported in our previous work [6–8]. Firstly, 100 mL dispersions were pumped into the visual chamber and heated to the desired temperature by an embedded electric heating system. The CO_2 was then bubbled into the chamber to achieve the desired pressure. Afterward, the surfactant dispersions and CO_2 were vigorously stirred at 1100 rpm for 3 min. Once agitation ceased, the V_{max} and $t_{1/2}$ were recorded by observing the foam height. All values were measured three times per experiment, and the average value was taken as the final result.

3.5. Characterization of Switchability of Aqueous Foams

To examine the switchability of aqueous foams produced from $UC_{22}AMPM$ and $UC_{18}AMPM$, the CO_2 and $NH_3 \cdot H_2O$ (25 vol.%) were used as triggers to "switch" foam on and off. First, at a 3 MPa CO_2 atmosphere, the aqueous foams were generated by the agitation of 100 mL of $UC_{22}AMPM$ and $UC_{18}AMPM$ aqueous dispersion at 1020 rpm for 3 min using an HTHP visualization foam meter, respectively. Subsequently, the appropriate amount of $NH_3 \cdot H_2O$ was introduced to the CO_2 aqueous foam system, during which the foaming and defoaming processes were tracked. This operation was repeated five times, and each cycle was separated by 10 min. All measurements were performed at 80 °C.

3.6. Rheological Test of Foaming Solution

The rheological measurements of the foaming solution were carried out on a Physica MCR 302 (Anton Paar, Graz, Austria) rotational rheometer equipped with a concentric cylinder geometry CC27. At atmospheric pressure, CO_2 was first bubbled into the sample at a flow rate of 200 ± 1 mL/min for 2 min. Then, 16 mL of previously gas-treated sample was introduced to the measuring cell and thermostatically incubated at the desired temperature for 20 min prior to experimentation. A solvent trap was used to reduce water evaporation in the experiments. For all experiments, flow curves were registered in a stress-controlled mode, and the data were acquired by the software Rheoplus TM. The temperature was finely controlled by a Peltier temperature control device.

4. Conclusions

In this work, we investigate comparatively the properties of CO_2 foams stabilized by $UC_{22}AMPM$ and $UC_{18}AMPAM$ and examined the evolution trend of foam properties concerning variation in external factors (i.e., temperature, pressure and salinity). The results showed that CO_2 aqueous foams prepared from $UC_{18}AMPM$ exhibited similar switching properties to $UC_{22}AMPM$, arising from their identical tertiary amine headgroups. However, due to the relatively long hydrophobic chain, $UC_{22}AMPM$ molecules self-assembled into wormlike micelles, but $UC_{18}AMPM$ cannot. The entanglement of these wormlike micelles into a transient network imparts high viscosity to the continuous phase of foam. During the foaming process, a large amount of liquid was transported into the foam liquid channels, forming the thicker foam film. Meanwhile, the high continuous phase viscosity of the foam system decelerates lamellae drainage. With lower drainage, the lamella remained thicker. The thicker films would enhance foam strength as well as hinder gas diffusion, arresting coalescence and Ostwald ripening, thereby enhancing the foam's lifetime. On the contrary, the viscosity of the $UC_{18}AMPM$ sample decreased to ~1.0 mPa·s because of the absence of wormlike micelles. The lower viscosity accelerated the drainage process, weakening the strength of the foam film. The reduced strength and thickness of foam film, in turn, led to the bursting of bubbles. As a result, $UC_{22}AMPM$ foam displayed better foaming ability and foam stability compared to $UC_{18}AMPAM$ foam under identical concentrations. More importantly, for $UC_{22}AMPM$-CO_2 foam, the positive influence derived from pressure and concentration on its foam properties is much more pronounced than those of its $UC_{18}AMPM$ counterpart. Compared with $UC_{18}AMPM$-CO_2 foam, the salinity and temperature had a relatively weak negative effect on the properties of $UC_{22}AMPM$-CO_2 foam. In summary, this comparative study advances mechanistic insights into the role of surfactant architecture in foam properties, as well as establishes macroscopic links among foam properties, surfactant structure and environmental factors, promoting the development of such foam systems.

Data Availability Statement: The data presented in this study are available on request from the corresponding author.

Conflicts of Interest: The authors declare no conflict of interest.

Sample Availability: Samples of the compounds including $UC_{22}AMPM$ and $UC_{18}AMPM$, are available from the authors.

References

1. Langevin, D. Aqueous foams: A field of investigation at the frontier between chemistry and physics. *Chemphyschem* **2008**, *9*, 510–522. [CrossRef]
2. Wei, P.; Guo, K.; Pu, W.; Xie, Y.; Huang, X.; Zhang, J. Aqueous Foam Stabilized by an in Situ Hydrophobic Polymer via Interaction with Alkyl Polyglycoside for Enhancing Oil Recovery. *Energy Fuels* **2020**, *34*, 1639–1652. [CrossRef]
3. Huang, Z.; Shuai, S.; Wang, H.; Liu, R.; Zhang, S.; Cheng, C.; Hu, Y.; Yu, X.; He, G.; Fu, W. Froth flotation separation of lepidolite ore using a new Gemini surfactant as the flotation collector. *Sep. Purif. Technol.* **2022**, *282*, 119122–119136. [CrossRef]
4. Sheng, Y.; Jiang, N.; Lu, S.; Wang, Q.; Zhao, Y.; Liu, X. Study of environmental-friendly firefighting foam based on the mixture of hydrocarbon and silicone surfactants. *Fire Technol.* **2020**, *56*, 1059–1075. [CrossRef]
5. Wang, J.; Nguyen, A.V.; Farrokhpay, S. Foamability of sodium dodecyl sulfate solutions: Anomalous effect of dodecanol unexplained by conventional theories. *Colloids Surf. A* **2016**, *495*, 110–117. [CrossRef]
6. Farajzadeh, R.; Krastev, R.; Zitha, P.L.J. Foam films stabilized with alpha olefin sulfonate (AOS). *Colloids Surf. A* **2008**, *324*, 35–40. [CrossRef]
7. Saint-Jalmes, A. Physical chemistry in foam drainage and coarsening. *Soft Matter* **2006**, *2*, 836–849. [CrossRef] [PubMed]
8. Wang, J.; Nguyen, A.V.; Farrokhpay, S. A critical review of the growth, drainage and collapse of foams. *Adv. Colloid Interface Sci.* **2016**, *228*, 55–70. [CrossRef]
9. Langevin, D. Aqueous foams and foam films stabilised by surfactants. Gravity-free studies. *C. R. Mécanique* **2017**, *345*, 47–55. [CrossRef]
10. Heerschap, S.; Marafino, J.N.; McKenna, K.; Caran, K.L.; Feitosa, K. Foams stabilized by tricationic amphiphilic surfactants. *Colloids Surf. A* **2015**, *487*, 190–197. [CrossRef]
11. Li, S.; Li, Z.; Wang, P. Experimental Study of the Stabilization of CO_2 foam by sodium dodecyl sulfate and hydrophobic nanoparticles. *Ind. Eng. Chem. Res.* **2016**, *55*, 1243–1253. [CrossRef]
12. Fukuoka, K.; Tomikawa, A.; Nakamura, Y.; Fujii, S. Aqueous foams stabilized with several tens of micrometer-sized polymer particles: Effects of surface hydrophilic–hydrophobic balance on foamability and foam stability. *Chem. Lett.* **2016**, *45*, 667–669. [CrossRef]
13. Pu, W.-F.; Wei, P.; Sun, L.; Jin, F.-Y.; Wang, S. Experimental investigation of viscoelastic polymers for stabilizing foam. *Ind. Eng. Chem. Ind. Ed.* **2017**, *47*, 360–367. [CrossRef]
14. Rouimi, S.; Schorsch, C.; Valentini, C.; Vaslin, S. Foam stability and interfacial properties of milk protein-surfactant systems. *Food Hydrocoll.* **2005**, *19*, 467–478. [CrossRef]
15. Murray, B.S.; Ettelaie, R. Foam stability: Proteins and nanoparticles. *Curr. Opin. Colloid Interface Sci.* **2004**, *9*, 314–320. [CrossRef]
16. Davis, J.P.; Foegeding, E.A. Comparisons of the foaming and interfacial properties of whey protein isolate and egg white proteins. *Colloids Surf. B* **2007**, *54*, 200–210. [CrossRef]
17. Stocco, A.; Rio, E.; Binks, B.P.; Langevin, D. Aqueous foams stabilized solely by particles. *Soft Matter* **2011**, *7*, 1260–1267. [CrossRef]
18. Binks, B.P.; Horozov, T.S. Aqueous foams stabilized solely by silica nanoparticles. *Angew. Chem. Int. Ed.* **2005**, *44*, 3722–3725. [CrossRef] [PubMed]
19. Schad, T.; Preisig, N.; Blunk, D.; Piening, H.; Drenckhan, W.; Stubenrauch, C. Less is more: Unstable foams clean better than stable foams. *J. Colloid Interface Sci.* **2021**, *590*, 311–320. [CrossRef]
20. Alzobaidi, S.; Da, C.; Tran, V.; Prodanovic, M.; Johnston, K.P. High temperature ultralow water content carbon dioxide-in-water foam stabilized with viscoelastic zwitterionic surfactants. *J. Colloid Interface Sci.* **2017**, *488*, 79–91. [CrossRef]
21. Wang, J.; Luo, X.; Rogers, S.; Li, P.; Feng, Y. Stabilization of CO_2 aqueous foams at high temperature and high pressure: Small-angle neutron scattering and rheological studies. *Colloids Surf. A* **2022**, *647*, 129015–129026. [CrossRef]
22. Chen, Y.; Elhag, A.S.; Worthen, A.J.; Reddy, P.P.; Ou, A.M.; Hirasaki, G.J.; Nguyen, Q.P.; Biswal, S.L.; Johnston, K.P. High Temperature CO_2-in-water foams stabilized with cationic quaternary ammonium Surfactants. *J. Chem. Eng. Data* **2016**, *61*, 2761–2770. [CrossRef]
23. Elhag, A.S.; Da, C.; Chen, Y.; Mukherjee, N.; Noguera, J.A.; Alzobaidi, S.; Reddy, P.P.; AlSumaiti, A.M.; Hirasaki, G.J.; Biswal, S.L.; et al. Viscoelastic diamine surfactant for stable carbon dioxide/water foams over a wide range in salinity and temperature. *J. Colloid Interface Sci.* **2018**, *522*, 151–162. [CrossRef]
24. Xue, Z.; Worthen, A.; Qajar, A.; Robert, I.; Bryant, S.L.; Huh, C.; Prodanovic, M.; Johnston, K.P. Viscosity and stability of ultra-high internal phase CO_2-in-water foams stabilized with surfactants and nanoparticles with or without polyelectrolytes. *J. Colloid Interface Sci.* **2016**, *461*, 383–395. [CrossRef] [PubMed]
25. Chu, Z.; Feng, Y. Vegetable-derived long-chain surfactants synthesized via a "Green" route. *ACS Sustain. Chem. Eng.* **2012**, *1*, 75–79. [CrossRef]
26. Feng, Y.; Chu, Z. A Facile route towards the preparation of ultra-long-chain amidosulfobetaine surfactants. *Synlett* **2009**, *2009*, 2655–2658. [CrossRef]
27. Zhang, P.; Bai, G.; Cui, G.; Zhang, L.; Peng, X.; Pei, S.; Ren, S. Enhanced CO_2 foam based on amide and amine surfactants and synergistically coupled with sodium dodecyl sulfate at high temperature and high pressure. *J. Pet. Sci. Eng.* **2019**, *179*, 266–275. [CrossRef]
28. Salonen, A.; In, M.; Emile, J.; Saint-Jalmes, A. Solutions of surfactant oligomers: A model system for tuning foam stability by the surfactant structure. *Soft Matter* **2010**, *6*, 2271–2281. [CrossRef]

29. Hu, X.; Li, Y.; He, X.; Li, C.; Li, Z.; Cao, X.; Xin, X.; Somasundaran, P. Structure-behavior-property relationship study of surfactants as foam stabilizers explored by experimental and molecular simulation approaches. *J. Phys. Chem. B* **2012**, *116*, 160–167. [CrossRef] [PubMed]

30. Fameau, A.-L.; Ventureira, J.; Novales, B.; Douliez, J.-P. Foaming and emulsifying properties of fatty acids neutralized by tetrabutylammonium hydroxide. *Colloids Surf. A* **2012**, *403*, 87–95. [CrossRef]

31. Oh, S.G.; Shah, D.O. Relationship between micellar lifetime and foamability of sodium dodecyl sulfate and sodium dodecyl sulfate/1-hexanol mixtures. *Langmuir* **1991**, *7*, 1316–1318. [CrossRef]

32. Petkova, B.; Tcholakova, S.; Chenkova, M.; Golemanov, K.; Denkov, N.; Thorley, D.; Stoyanov, S. Foamability of aqueous solutions: Role of surfactant type and concentration. *Adv. Colloid Interface Sci.* **2020**, *276*, 102084–102103. [CrossRef] [PubMed]

33. Sun, Y.; Qi, X.; Sun, H.; Zhao, H.; Li, Y. Understanding about How Different Foaming Gases Effect the Interfacial Array Behaviors of Surfactants and the Foam Properties. *Langmuir* **2016**, *32*, 7503–7511. [CrossRef] [PubMed]

34. Zhou, H.; Qu, C.; Lu, G.; Li, Z.; Wang, X.; Yin, H.; Feng, Y. Deliquification of low-productivity natural gas wells with in situ generated foams and heat. *Energy Fuels* **2021**, *35*, 9873–9882. [CrossRef]

35. Wang, J.; Liang, M.; Tian, Q.; Feng, Y.; Yin, H.; Lu, G. CO_2-switchable foams stabilized by a long-chain viscoelastic surfactant. *J. Colloid Interface Sci.* **2018**, *523*, 65–74. [CrossRef] [PubMed]

36. Dehdari, B.; Parsaei, R.; Riazi, M.; Rezaei, N.; Zendehboudi, S. New insight into foam stability enhancement mechanism, using polyvinyl alcohol (PVA) and nanoparticles. *J. Mol. Liq.* **2020**, *307*, 112755–112768. [CrossRef]

37. Pang, Z.; Wu, Y.; Zhao, M. Novel evaluation method of foam agents for thermal recovery in heavy oil Reservoirs. *Energy Fuels* **2016**, *30*, 2948–2957. [CrossRef]

38. Hill, C.; Eastoe, J. Foams: From nature to industry. *Adv. Colloid Interface Sci.* **2017**, *247*, 496–513. [CrossRef] [PubMed]

39. Feng, D.; Zhang, Y.; Chen, Q.; Wang, J.; Li, B.; Feng, Y. Synthesis and surface activities of amidobetaine surfactants with ultra-long unsaturated hydrophobic chains. *J. Surfactants Deterg.* **2012**, *15*, 657–661. [CrossRef]

40. Wang, J.; Feng, Y.; Agrawal, N.R.; Raghavan, S.R. Wormlike micelles versus water-soluble polymers as rheology-modifiers: Similarities and differences. *Phys. Chem. Chem. Phys.* **2017**, *19*, 24458–24466. [CrossRef]

41. Zhang, Y.; Chu, Z.; Dreiss, C.A.; Wang, Y.; Fei, C.; Feng, Y. Smart wormlike micelles switched by CO_2 and air. *Soft Matter* **2013**, *9*, 6217–6221. [CrossRef]

42. Langevin, D. On the rupture of thin films made from aqueous surfactant solutions. *Adv. Colloid Interface Sci.* **2020**, *275*, 102075–102084. [CrossRef]

43. Qu, C.; Wang, J.; Yin, H.; Lu, G.; Li, Z.; Feng, Y. Condensate oil-tolerant foams stabilized by an anionic-sulfobetaine surfactant mixture. *ACS Omega* **2019**, *4*, 1738–1747. [CrossRef]

44. Fan, C.; Jia, J.; Peng, B.; Liang, Y.; Li, J.; Liu, S. Molecular dynamics study on CO_2 foam films with sodium dodecyl sulfate: Effects of surfactant concentration, temperature, and pressure on the interfacial tension. *Energy Fuels* **2020**, *34*, 8562–8574. [CrossRef]

45. Maiti, K.; Mitra, D.; Guha, S.; Moulik, S.P. Salt effect on self-aggregation of sodium dodecylsulfate (SDS) and tetradecyltrimethy-lammonium bromide (TTAB): Physicochemical correlation and assessment in the light of Hofmeister (lyotropic) effect. *J. Mol. Liq.* **2009**, *146*, 44–51. [CrossRef]

46. Kumar, B.; Tikariha, D.; Ghosh, K.K. Effects of Electrolytes on Micellar and Surface Properties of Some Monomeric Surfactants. *J. Dispers. Sci. Technol.* **2012**, *33*, 265–271. [CrossRef]

47. McCoy, T.M.; Valiakhmetova, A.; Pottage, M.J.; Garvey, C.J.; Campo, L.; Rehm, C.; Kuryashov, D.A.; Tabor, R.F. Structural Evolution of Wormlike Micellar Fluids Formed by Erucyl Amidopropyl Betaine with Oil, Salts, and Surfactants. *Langmuir* **2016**, *32*, 12423–12433. [CrossRef]

48. Parker, A.; Fieber, W. Viscoelasticity of anionic wormlike micelles: Effects of ionic strength and small hydrophobic molecules. *Soft Matter* **2013**, *9*, 1203–1213. [CrossRef]